



***In situ* interactive characteristics of reactive minerals in soil colloids and soil carbon preservation differentially revealed by nanoscale secondary ion mass spectrometry and X-ray absorption fine structure spectroscopy**

Jian Xiao¹, Xinhua He², Ying Zhou³, Lirong Zheng⁴, Jialong Hao⁵, Wei Ran¹, Qirong Shen¹,

5 **Guanghai Yu^{1,6,*}**

¹ National Engineering Research Center for Organic-based Fertilizers, Jiangsu Collaborative Innovation Center for Solid Organic Waste Resource Utilization, Jiangsu Provincial Key Lab for Organic Solid Waste Utilization, Nanjing Agricultural University, Nanjing 210095, China

² School of Plant Biology, University of Western Australia, Crawley, WA 6009, Australia

10 ³ Shanghai Institute of Measurement and Testing Technology, Shanghai 201203, China

⁴ Beijing Synchrotron Radiation Facility, Institute of High Energy Physics, Chinese Academy of Sciences, Beijing 100049, China

⁵ Key Laboratory of Earth and Planetary Physics, Institute of Geology and Geophysics, Chinese Academy of Science, Beijing 100029, China

15 ⁶ Department of Plant Pathology, North Carolina State University, Raleigh, NC 27695, USA.

* Correspondence to: G. H. Yu (yuguanghai@njau.edu.cn or gyu6@ncsu.edu)



Abstract. Mineral binding is a major mechanism for soil carbon (C) stabilization. However, the submicron information about the *in situ* mechanisms of different fertilization practices affecting organo-mineral complexes and associated C preservation remains unclear. Here, we applied nano-scale secondary ion mass spectrometry (NanoSIMS), X-ray photoelectron spectroscopy (XPS), and X-ray absorption fine structure spectroscopy (XAFS) to examine differentiating effects of inorganic versus organic fertilization on interactions between highly reactive minerals and soil C preservation. To examine such interactions, soils and their extracted colloids were collected during a 24-year long-term fertilization period (1990-2014) (no-fertilization, Control; chemical nitrogen (N), phosphorus (P) and potassium (K) fertilization, NPK; and NPK plus swine manure fertilization, NPKM). The results for different fertilization conditions showed a ranked soil organic matter (SOM) concentration with NPKM > NPK > Control. Meanwhile, oxalate extracted Al (Al_o), Fe (Fe_o), short range ordered (SRO) Al (Al_{xps}), Fe (Fe_{xps}), and dissolved organic carbon (DOC) ranked with NPKM > Control > NPK, but ratios of DOC/ Al_{xps} and DOC/ Fe_{xps} ranked with NPKM > NPK > Control. Compared with the NPK treatment, NPKM treatment enhanced the C binding loadings of Al and Fe minerals in soil colloids at the submicron scale. Furthermore, a greater concentration of highly reactive Al and Fe minerals was present under NPKM than under NPK. Together, these submicron scale findings suggest that both reactive mineral species and their associations with C are differentially affected by inorganic and organic fertilization.

Key words: Al and Fe minerals; inorganic and organic fertilization; organo-mineral complexes; reactive minerals; carbon binding capability; X-ray photoelectron spectroscopy (XPS)



1. Introduction

Associations of organic matter (OM) with pedogenic minerals, which are termed as organo-mineral
40 complexes, are known to be key controls in the biogeochemical processes that retain OM in natural soil
system (Torn et al., 1997; Kögel-knbaner et al., 2008; Mikutta et al., 2009; Schmidt et al., 2011). Soil
OM (SOM) preferentially binds to rough surfaces, which provide a multitude of reactive mineral
surfaces (Kögel-Knabner et al., 2008; Chen et al., 2014; Vogel et al., 2014). These reactive minerals are
also termed as short-range ordered (SRO) meta-stable colloidal minerals in volcanic ejecta (Torn et al.,
45 1997), and serve as the nuclei for soil organic carbon (SOC) storage (Hochella et al., 2008;
Kögel-Knabner et al., 2008; Remusat et al., 2012; Vogel et al., 2014). Therefore, reactive Al and Fe
minerals in soil play a critical role in determining C stability (Solomon et al., 2012; Hernes et al., 2013).

On the other hand, the reactive mineral surface of organo-mineral complexes in the complex soil
matrix (mainly the top-soil layer) could be greatly improved through organic amendments to soil, such
50 as the anthropogenic importation of organic fertilizers under long-term experimentation (Schmidt et al.,
2011; Hernandez et al., 2012; Yu et al., 2012; Wen et al., 2014a; Abdala et al., 2015). However, little is
known about the effects of different fertilization practices on the *in situ* associations between reactive
minerals and SOC in soil colloids at a submicron scale. Meanwhile, there is few evidence demonstrating
that the *in situ* preservation capacity of reactive minerals on SOC. In general, *in situ* investigations of
55 natural organo-mineral complexes are restricted to bulk analyses of operationally defined physical
fractions (Hatton et al., 2012 and 2015; Remusat et al., 2012; Vogel et al., 2014). In contrast, techniques
for direct visualization at the submicron scale could greatly aid in gaining a better understanding of the



interactions between organic structures and reactive minerals (Remusat et al., 2012; Vogel et al., 2014; Xiao et al., 2015). For instance, nano-scale secondary ion mass spectrometry (NanoSIMS) has the
60 potential to examine the spatial integrity of soil microenvironments and has been designed for high lateral resolution (down to 50 nm) imaging, while still maintaining high mass resolution and high sensitivity (mg kg^{-1} range) (Herrmann et al., 2007; Xiao et al., 2015). Previous studies have shown that NanoSIMS is an effective technique for studying natural organo-mineral complexes at the submicron scale (Herrmann, 2007; Mueller et al., 2012; Remusat et al., 2012; Hatton et al., 2012 and 2015; Vogel
65 et al., 2014). High-resolution transmission electron microscopy (HRTEM) combined with selected area electron diffraction (SAED) is also a promising technique that can provide detailed information on organo-mineral surfaces, as well as changes in their surface chemistries (Wen et al., 2014a; Yaron-Marcovich et al., 2005). Although direct observations of organo-mineral complexes by NanoSIMS and HRTEM have been previously described (Ramos et al., 2013; Vogel et al., 2014; Rumpel et al., 2015), few studies have reported the effects of fertilization practices on the
70 organo-mineral complexes in soil colloids. In addition, X-ray photoelectron spectroscopy (XPS) can identify the oxidation state of elements on the surface (2~10 nm) of minerals (Zhu et al., 2014). Compared with XPS technique, X-ray absorption fine structure spectroscopy (XAFS) is a powerful tool for both identification and quantification of different mineral phases present in soil colloids (Li et al.,
75 2015; Xiao et al., 2015).

Using soil colloids extracted from 24-year fertilized soils (1990-2014), the objectives of this study were to address 1) the effects of fertilization practices on the quantity and composition of Al and Fe



minerals, and 2) the *in-situ* interactions between SOC and minerals at the submicron scale.

2. Materials and methods

80 2.1. Soil samples

Samples of soil (Ferralic Cambisol, FAO soil taxonomic classification) were from a long-term (1990-2014) fertilization site in Qiyang, Hunan, Southern China (26°45'N, 111°52'E, 120 m above sea level). The long-term fertilization experiment, which belongs to the Institute of Agricultural Resources and Regional Planning, Chinese Academy of Agricultural Sciences, has been under an annual rotation
85 of wheat and corn cropping system since September 1990. The topsoil contained 61.4% clay, 34.9% silt and 3.7% sand. Three fertilization treatments with 2 replicates or plots (20 m × 10 m) for each treatment were examined as follows: 1) no fertilization (Control), 2) chemical nitrogen (N), phosphorus (P) and potassium (K) (NPK) and 3) a combination of the chemical fertilizers with swine manure (NPKM) (see Fig. S1 for detailed fertilization rates). The NPK and MNPK had the same total application of 300 kg N
90 ha⁻¹ yr⁻¹. The applied N was 100% urea in the NPK, but was 30% from urea with the remaining 70% from swine manure in the MNPK. A 1.0-m-deep cement buffer zone was constructed between each plot. Each soil sample was a composite of twenty random cores (5 cm internal diameter auger) collected at 0-20 cm depth from one replicate plot. The fresh soil was mixed thoroughly, air-dried, and sieved (5 mm) for further analyses.

95 2.2. Soil colloids extraction and quantitation of highly reactive Al and Fe minerals

The soil colloids extraction was based on a previously described method (Schumacher et al., 2005). Briefly, 100 g of fresh soils was suspended in 500 mL of deionized water on a horizontal shaker (170



rpm) for 8 hr at $25 \pm 1^\circ\text{C}$, and centrifuged at 2500 g for 6 min (Fig. S1). Aliquots of the supernatant suspensions and freeze-dried soil colloid samples were then generated. Quantitation of highly reactive
100 minerals, including Al and Fe minerals (Al_o , Fe_o), was performed using the acid ammonium-oxalate extraction method (Kramer et al., 2012). In brief, soil was extracted using 0.275 M ammonium oxalate at pH 3.25 with a 1:100 soil:extractant (w/v) ratio. Ammonium oxalate was used to selectively remove short-range ordered hydrous oxides of Fe and Al such as allophane and ferrihydrite.

2.3. HRTEM analysis

105 HRTEM samples were prepared by dropping soil mobile colloids onto carbon coated copper grids. The images were recorded at an acceleration voltage of 200 keV using a JEOL JEM-2100F microscope (JEOL JEM-2100F, Japan), which was at the Analysis and Testing Centre of Nanjing Normal University, China. HRTEM images, selected area electron diffraction (SAED) and energy dispersive X-ray analysis (EDX) were conducted using the JEOL JEM-2100F microscope to characterize soil
110 colloid samples.

2.4. NanoSIMS analyses

For NanoSIMS measurements, several aliquots of the colloidal suspension from these three different fertilization treatments were separately dropped onto a silicon wafer and air-dried. In this study, we chose 6 spots from the NanoSIMS images to show the replicates of each soil colloid sample because
115 the majority of particulate organo-mineral complexes were included and similar according to the characterization of natural colloids (Philippe and Schaumann, 2014; Xiao et al., 2015). For every sample, all 6 spots were analyzed to obtain a reliable data basis for the calculation of the fate of ^{12}C ,



$^{27}\text{Al}^{16}\text{O}^-$, and $^{56}\text{Fe}^{16}\text{O}^-$ (Table S2).

The analyses were performed on a NanoSIMS 50L (Cameca, Gennevilliers, France) instrument at
120 the Institute of Geology and Geophysics, Chinese Academy of Sciences, China. Prior to analysis, the
gold coating layer (30 nm) and any possible contamination of the sample surface were sputtered using a
high primary beam current (pre-sputtering). During the pre-sputtering, the reactive Cs^+ ions were
implanted into the sample to enhance the secondary ion yields. The primary beam (~ 0.9 pA) focused at
a lateral resolution of 100-200 nm, was scanned over the samples, and the secondary ion images of $^{12}\text{C}^-$,
125 $^{27}\text{Al}^{16}\text{O}^-$, and $^{56}\text{Fe}^{16}\text{O}^-$ were simultaneously collected by electron multipliers with an electronic dead
time fixed at 44 ns. The presence of $^{12}\text{C}^-$ ion mass indicated SOC, while the presence of $^{27}\text{Al}^{16}\text{O}^-$ and
 $^{56}\text{Fe}^{16}\text{O}^-$ demonstrated Al and Fe minerals, respectively. The estimated depth resolution using 16 keV
 Cs^+ ions as the primary ion beam was about 15 nm. We compensated for the charging due to the
non-conductive mineral particles using the electron flood gun of the NanoSIMS instrument. All
130 measurements were conducted in an imaging mode. The dwell time was 1 ms pixel^{-1} for all acquisitions.
Specific details describing NanoSIMS measurements can be found in previous publications (Vogel et al.,
2014; Xiao et al., 2015).

The analyses were carried out on different cluster compositions using Image J software with the
OpenMIMS plugin (http://www.nrims.hms.harvard.edu/NRIMS_ImageJ.php). In this study, regions of
135 interest (ROIs) were selected according to the intensity of the secondary $^{12}\text{C}^-$ ion mass. Specifically, the
visible SOC surface areas were divided into rich and less rich $^{12}\text{C}^-$ ROIs according to the pixel value
extracted from the NanoSIMS images. The $^{12}\text{C}^-$ rich ROIs included the areas above 90 pixels and the



¹²C⁻ less rich ROIs included the areas in the range of 90-40 pixels under Control and NPK, while the ¹²C⁻ rich ROIs were above 50 pixels and the ¹²C⁻ less rich ROIs were in the range of 50-30 pixels under NPKM. The threshold option of the Image J software was used to automatically generate the ROIs from these NanoSIMS images. In doing so, the triangle algorithm was used (Vogel et al., 2014; Xiao et al., 2015). The ROIs of the ²⁷Al¹⁶O⁻ and ⁵⁶Fe¹⁶O⁻ images were combined afterwards to obtain the ROIs according to the distribution of the ¹²C⁻ rich ROIs and ¹²C⁻ less rich ROIs under different fertilizations conditions (Table S2).

145 2.5. XPS analyses

The sample preparation for the XPS procedures was adapted from Gerin et al. (2003). The XPS data were collected using a PHI 5000 Versa Probe X-ray photoelectron spectrometer (UIVAC-PHI, Japan) equipped with a monochromatized Al K α X-ray source (1486.69 eV). The binding energy scale was corrected using the adventitious hydrocarbon C 1s spectrum (C 1s = 284.6 eV) (Zhu et al., 2014). The analyzed zone corresponded to a 300 μ m \times 300 μ m elliptical spot. The surface charge induced by the photo ejection process was balanced using a flood gun at 6 eV. To optimize the signal to noise ratio, spectra were recorded at a detector resolution corresponding to 0.125 eV per channel. The base pressure in the spectrometer was 6.7×10^{-10} Torr. The XPS data analyses were performed using XPSPEAK 4.1 with Shirley background correction, as referenced at <http://www.lasurface.com/xps/index> and <http://srdata.nist.gov/xps/Default.aspx>. No fixed full width at half maximum (FWHM) values were determined for the spectra of soil colloids collected under contrasting fertilization treatments. Gaussian-Lorentzian ratios were freely fit for all peaks in this study (Liang et al., 2008).



2.6. XAFS spectra analyses

Fe K-edge X-ray absorption fine structure (XANES) and extended X-ray absorption fine structure
160 (EXAFS) spectra were recorded at the beamline 1W1B at the XAFS Station of the Beijing Synchrotron
Radiation Facility (BSRF, Beijing, China) using a Si (111) double-crystal monochromator. The storage
ring was operated at 2.5 GeV with the electron current decreasing from 240 to 160 mA within
approximately 8 hrs. Samples were ground into fine powders and brushed onto tapes, which were then
stacked together to yield approximately one X-ray-absorption length at their corresponding metal edges.
165 The intensities of incident and transmitted X-rays were monitored by ionization chambers filled with
nitrogen gas. All reported spectra were measured at 20°C. Spectra were collected in quick-scan and
transmission mode. XANES spectra were recorded with 0.5 eV step, counting 10 s from 7,100 to 7,250
eV. EXAFS spectra were recorded up to $k = 14.0 \text{ \AA}^{-1}$, using 1 eV steps and counting for 100–200 s per
scan. To improve data quality, 5 XANES scans and 5 EXAFS scans were recorded for each sample. The
170 X-ray energy scale was calibrated to the iron K-edge (7112.0 eV) using an iron metal foil prior to XAFS
acquisition. The incident X-ray energy varied from 7100 to 7800 eV in 0.5 eV increments using a
monochromator (dwell time = 10 s). Averaged spectra were normalized using Athena (Version 2.1.1,
California, USA) software, and EXAFS data were extracted using the Autoback routine, using the same
program. Linear combination fitting (LCF) of XANES data were performed with the respective
175 functions of Athena. EXAFS data were Fourier Transformed by applying a Kaiser-Bessel window with
a Bessel-weight of 3.0. The Fe K-edge XANES spectra with LCF of eight standard iron samples were
used to precisely characterize the composition of Fe minerals (Baumgartner et al., 2013; Senn et al.,



2015). The standard iron samples of ferrous sulfate, ferrous oxalate, ferric sulfate, ferric oxalate, goethite, hematite, ferrihydrite, and maghemite were also recorded in transmission mode, which were
180 purchased or synthesized (Table S3).

2.7. Chemical analyses

The concentration of SOC was quantified using a CN analyzer (Vario EL, Elementar GmbH, Hanau, Germany), while SOM was $1.724 \times \text{SOC}$. Soil pH was determined using a pH electrode at a 1:5 soil: distilled water ratio. The concentration of Fe and Al was quantified by inductively coupled plasma
185 atomic emission spectroscopy (710/715 ICP-AES, Agilent, Australia). The concentration of DOC was determined by a TOC/TN analyzer (multi N/C 3000, Analytik Jena AG, Germany).

2.8. Statistical analyses

One-way analysis of variance (ANOVA) was used to test the effects of long-term fertilization on reactive iron minerals in the soil. Significant differences between treatments (means \pm SE, $n = 3$) were
190 determined by Tukey's HSD post hoc test at $P < 0.05$, where the conditions of normality and homogeneity of variance were met.

3. Results

3.1. Concentration and morphology of organo-mineral complexes in soil colloids under contrasting fertilizations

195 Compared with a soil pH of 5.47 under Control, the soil pH significantly decreased to 4.15 under NPK but significantly increased to 5.84 under NPKM (Table 1). SOM concentrations in different fertilization treatments ranked as $\text{NPKM} > \text{NPK} > \text{Control}$ (Table 1). Oxalate extracted Al (Al_o), Fe



(Fe_o), SRO Al (Al_{xps}), Fe (Fe_{xps}), and DOC ranked as NPKM > Control > NPK, but ratios of DOC/Al_{xps} and DOC/Fe_{xps} ranked as NPKM > NPK > Control (Table 1).

200 To get insight into the spatial distribution of SOM associated with reactive mineral particles, we used both HRTEM and NanoSIMS to acquire *in situ* observations of such associations. At the nanometer scale, the HRTEM images of extracted soil colloids provided direct visualization of the presence of soil SRO minerals from Control-, NPK- and NPKM-fertilized samples (Fig. 1). Soil minerals showed amorphous and crystalline patterning in different regions (Fig. 1-a, b). The SAED
205 (selected area electron diffraction) pattern further demonstrated that the amorphous mineral species were dominated by Al, Si, and O, while the crystalline minerals were mainly composed of Fe and O (Fig. 1-c, d).

The NanoSIMS images of ¹²C⁻, ²⁷Al¹⁶O⁻, and ⁵⁶Fe¹⁶O⁻ ion masses showed the submicron elemental distribution in soil colloids (Fig. 2). Under different fertilizations, organo-mineral complexes also
210 distributed in a heterogeneous way as indicated by the color bar on the NanoSIMS images (from blue to white) at the submicron scale (Figs. 2 and S2).

3.2. Binding capability of C by Al and Fe minerals

We next used the region of interests (ROIs) to explore the C binding capability of Al and Fe minerals. Based on the pixel value of secondary ¹²C⁻ ion mass in all spots from each sample, the
215 selected ROIs were identified. The selected ROIs were further divided into ¹²C⁻ rich- and ¹²C⁻ less rich- ROIs (Fig. S2 and Table S2). The area percentage of the ¹²C⁻ rich- or ¹²C⁻ less rich- ROIs accounted for 7.47 or 40.18 %, 10.80 or 27.64 % and 8.23 or 37.99% under Control, NPK and NPKM, respectively



(Table S2). Interestingly, the box plots (Fig. 3) of $^{12}\text{C}/^{27}\text{Al}^{16}\text{O}^-$ (a, b) and $^{12}\text{C}/^{56}\text{Fe}^{16}\text{O}^-$ (c, d) ratios showed that both the median and the mean value were higher under NPKM than under NPK. These results suggest that more organic C may be bound by Al and Fe minerals under NPKM than under NPK (Figs. 2 and 3).

3.3. Chemical speciation of reactive minerals and C

The XPS Al $2p_{3/2}$ peak-fitting results (Table 2 and Fig. 4) showed that 45% allophane (~73.80 eV), 29.4% of boehmite (~74.5 eV) and 26% Al Ox (~75.40 eV) were present in soil colloids under NPKM. In contrast, approximately 43% and 34% of allophane were observed in soil colloids under NPK and Control, respectively. Considering higher (over 5 times) total Al concentrations in soil colloids under NPKM than NPK (Table 1), the amount of allophane in soil colloids under NPKM is approximately 5 times higher than that of NPK.

Linear combination fitting (LCF) of soil colloids (Fig. 5 and Table 3) showed that goethite (56.8%-67.0%) and hematite (14.9%-25.0%) were prominent under all three fertilizations. The remaining Fe phases were composed of the less crystalline ferrihydrite species. The percentage of ferrihydrite was the highest under NPKM ($18.0 \pm 0.02\%$), followed by Control ($16.0 \pm 0.03\%$) and NPK ($6.30 \pm 0.02\%$). In view of the better C binding and potential preservation capability of ferrihydrite when compared to goethite and hematite (Baker et al., 2010; Kramer et al., 2012; Lalonde et al., 2012; Xiao et al., 2015), it is reasonable to conclude that there is greater C loading by Fe minerals under organic fertilization than under chemical fertilization.



Furthermore, Fe K-edge EXAFS was used for qualitative analysis of the composition of Fe minerals in soil colloids. The Fe k^3 -weighted EXAFS spectra (Fig. 6, left) showed that the spectral features of soils colloids under Control and NPKM were more similar to those of goethite, hematite, and ferrihydrite than to other minerals or compounds, suggesting that those Fe minerals are mainly composed of goethite, hematite, and ferrihydrite. The spectral features of the soils under NPK were more similar to those of goethite and hematite than to those of other minerals or compounds, supporting that those Fe minerals are mainly composed of goethite and hematite rather than short-range ordered ferrihydrite. Specifically, the EXAFS of Fe oxides showed double antinodes at 9.2 and 11.6 \AA^{-1} under Control and NPKM, whereas triple antinodes were observed under NPK at 9.2, 10.3 and 11.6 \AA^{-1} (Fig. 6, left). Double antinodes were found in hematite and ferrihydrite, whereas triple antinodes were observed in goethite. These results implied that the coordination environment for Fe-Fe linkages in Control and NPKM samples might be different from that in NPK samples because the observed peak primarily derived from the Fe-Fe coordination in goethite (Mitsunobu et al., 2012).

Fourier transforms showed that Fe minerals under Control and NPKM had most of the features observed in goethite, hematite, and ferrihydrite [i.e., first peak (Fe-O) and second peak (edge-sharing Fe-Fe)] and amplitude of multiple-scattering peak at 5.2 \AA . Specifically, the first shell at 1.5 \AA corresponds to the Fe-O coordination, and the intensity and position were approximately identical between the Control or NPKM treated soil colloids and ferrihydrite spectra. In contrast, the second shell identified at $R + \Delta R = 2.3\text{-}3.5 \text{\AA}$ corresponding to the Fe-Fe coordination was smaller than that of



ferrihydrate. These results indicated that Fe in the Control and NPKM treated soil colloids might have a weaker Fe-Fe linkage than that in ferrihydrate.

In addition, the XPS C 1s peak-fitting results (Table 2 and Fig. 4) demonstrated that aromatic C (Ar-C-C/Ar-C-H, ~284.6 eV) was dominant under all three fertilizations, with the highest percentage (75.86%) under NPKM, followed by NPK (62.51%) and Control (62.26%). In contrast, percentages of other carbon groups, i.e., ether or alcohol carbon (C-O) and ketone or aldehyde carbon (C=O), were lowest under NPKM among the three contrasting fertilization treatments.

4. Discussion

4.1. Long-term organic fertilization increased the concentration of highly reactive Al and Fe minerals and their soil C binding capacity

Organic fertilization has been shown to facilitate the formation of highly reactive Al and Fe minerals according to quantitative chemical analyses (Yu et al., 2012; Wen et al., 2014a, b; Wu et al., 2014; Huang et al., 2016), but the direct potential of C preservation capacity by Al and Fe minerals under different fertilizations regimes remains unexplored. In this study, the ROI analyses of NanoSIMS *in situ* observation (Fig. 3) provided direct evidence that long-term organic fertilization strengthened the SOC binding and preservation capability of Al and Fe minerals in soil colloids as well as a highly spatial heterogeneity of soil colloids at the submicron scale. Additionally, colloids from the NPKM treated soil had higher ratios of DOC/Al_{xps} and DOC/Fe_{xps} than those under Control and NPK (Table 1), which was compatible with the assumption suggested by the NanoSIMS and HRTEM. These results could be derived from a long-term continuous organic C input that might have enriched soil microbial



communities and then in turn supported an efficient formation of the concomitant organo-mineral aggregates (Wild et al., 2014; Basler et al., 2015).

Moreover, it was notable that greater amounts of aromatic C were observed under NPKM than under NPK or Control, which indicated that additional aromatic functional groups had been attached to highly reactive Al and Fe minerals under NPKM. This result is also supported by C 1s near-edge X-ray fine structure (NEXAFS) spectroscopy that compared to the NPK treatment, the NPKM treatment markedly increased the percentages of both the aromatic (283.0–286.1 eV) and phenolic (286.2–287.5 eV) groups over 2.8-fold (Huang et al., 2016). Since aromatic compounds are preferentially retained at the interface of reactive minerals and that long-term C storage by SRO minerals has occurred via the mechanism of chemical retention with dissolved aromatic acids (Kramer et al., 2012).

4.2. Long-term organic fertilization modified the composition of highly reactive Al and Fe minerals

Our results from both XPS and Fe K-edge XAFS showed that organic fertilization facilitated the formation of highly reactive Al and Fe minerals, e.g., allophane, imogolite, and ferrihydrite (Tables 2-3 and Figs. 4-6), which could further explain why long-term organic manure fertilization was able to alter the C and N binding capacity of Al and Fe minerals. The data from the TOC and ICP-AES (Table 1) also supported that soils under NPKM contained significantly higher percentages of Al_o, Fe_o, SRO minerals, and SOM than those under NPK. The results from HRTEM and SAED (Fig. 1) further showed that soil colloids under NPKM were composed of large amounts of meta-stable amorphous or SRO minerals (e.g., allophane, imogolite and ferrihydrite), which could form stable organic-mineral bonds



through anion and inner-sphere ligand-exchange reactions and would thus be well-suited to physically protecting geometries (Torn et al., 1997; Yu et al., 2012; Basler et al., 2015). These results are consistent with previous studies using ^{27}Al nuclear magnetic resonance (NMR) spectroscopy and Fourier-transform infrared spectroscopy (FTIR) (Yu et al., 2012; Wen et al., 2014a,b; Wu et al., 2014). By using
300 Fe K-edge XANES spectroscopy, Huang et al. (2016) also showed that reactive Fe minerals were mainly composed of less crystalline ferrihydrite in the M-treated soil and more crystalline goethite in the NPK-treated soil. Furthermore, high amounts of organic acid in NPKM fertilized soils may play a critical role in promoting the formation of reactive minerals (Huang et al., 2016).

In addition, studies have shown that the formation of highly reactive Al and Fe minerals could
305 greatly benefit the binding and potential preservation of SOC (Torn et al., 1997; Wen et al., 2014a; Xiao et al., 2015). Especially, reactive Fe minerals may responsible for the retention of aromatic C and O-alkyl C in soils (Huang et al., 2016). Under favorable conditions, SOC turnover in soil colloids with highly reactive Al and Fe minerals could persist in tephra beds for at least 250,000 yrs (Parfitt, 2009). Accumulation of highly reactive Al and Fe minerals in soil colloids could therefore improve SOC
310 sequestration under long-term organic manure fertilization. Furthermore, soil colloids usually consist of mixtures or complexes of hydrous oxides of Fe, Al and natural organic matter, which have important implications for deposition, aggregation, and sorption processes (Schumacher et al., 2005; Herrmann et al., 2007; Mueller et al., 2012).

4.3. Environmental implications and technical challenges

315 Soils are highly complex materials that are structurally and elementally heterogeneous across a



wide range of spatial and temporal scales (Herrmann et al., 2007; Mueller et al., 2012; Vogel et al., 2014). In porous media the stability, transport, and deposition of colloids, which usually consist of mixtures or complexes of hydrous oxides of Fe, Al, and natural organic matter, are strongly affected by the mobilized colloidal particles and specific surface area (Kaiser and Guggenberger, 2003; Schumacher et al., 2005). By combining HRTEM, NanoSIMS, XPS and/or XANES technique, the present study investigated the previously unknown highly reactive mineral elements and their spatial distribution patterns under contrasting fertilizations. This strategy has the following key advantages: HRTEM, NanoSIMS images and elemental mapping with sufficient resolution are able to illustrate the specific relationship and spatial heterogeneity of organic, highly reactive mineral complexes under contrasting fertilizations, while decomposition of XPS and Fe K-edge XANES peaks to definite semi-quantitative determinations shows the elemental valence states and compositions. Nevertheless, we are still faced with the challenge of how to utilize spatial information to parameterize models for handling the complex, stochastic interactions between organo-mineral complexes and their microenvironments, including a range of biogeochemical transformation influenced by different fertilization treatments at the submicron scale (Remusat et al., 2012; Abdala et al., 2015; Hatton et al., 2015). Because of the highly heterogeneous distribution of mineral elements/C-functional groups in soils, investigation on more regions in more samples is necessary to obtain solid relationships between organic C and mineral elements using the NanoSIMS *in situ* observation. Meanwhile, inadequate sample preparation to avoid artefacts is also a challenge, which may introduce a bias in the interpretation of NanoSIMS data and location of regions-of-interest (Herrmann et al., 2007). In addition, the complexity of iron chemistry in



soils also makes Fe XANES and EXAFS characterization a challenge. For example, the accuracy of the LCF results is strongly affected by the correctness of the applied set of predictor variables (Prietz et al., 2007). And EXAFS only provides average structural information over a short-range order, therefore it fails to determine if the minerals are crystalline or amorphous (Li et al., 2015), which is important in understanding the stabilization of organic carbon. With the enough soil samples and the improvement of sample preparation, these limitations can be well overcome, and the strategy is expected to receive wide applications in the fields of environmental science.

5. Conclusions

In this study, we showed that long-term (1990-2014) organic fertilization increased the carbon binding loading and the potential preservation capacity of soil colloids through the formation of highly reactive Al and Fe minerals. Meanwhile, the organo-mineral complexes in the colloids extracted from fertilized soils showed the highly spatial heterogeneity at the submicron scale. The quantities of highly reactive Al minerals (allophane, imogolite) and highly reactive Fe minerals (ferrihydrite) were significantly higher under NPKM than under Control and NPK. Our results demonstrated that the combination of nano-scale secondary ion mass spectrometry (NanoSIMS) and X-ray absorption fine structure spectroscopy (XAFS) is a promising approach to distinguish relationships between C preservation and minerals in natural soil colloids as well as the potential for SOM accumulation under inorganic and organic fertilizations at the submicron scale.

Supplementary material related to this article is available online at:

<http://www.biogeosciences.net/>



Acknowledgment. The authors thank B.R. Wang for his assistance in soil sampling in the Qiyang Long-term Fertilization Station. This work was jointly financially supported by National Natural Science Foundation of China (41371248 and 41371299), Natural Science Foundation of Jiangsu Province of China (BK20131321), the Qing Lan Project, the Innovative Research Team Development
360 Plan of the Ministry of China (IRT1256), the 111 Project (B12009), the Priority Academic Program Development (PAPD) of Jiangsu Higher Education Institutions, and Research Project of Shanghai Municipal Bureau of Quality and Technical Supervision (I00RJ1414).

References

- Abdala, D.B., da Silva, I.R., Vergutz, L., and Sparks, D.L.: Long-term manure application effects on
365 phosphorus speciation, kinetics and distribution in highly weathered agricultural soils, *Chemosphere*, 119, 504-514, 2015.
- Baker, L.L., Strawn, D.G., Vaughan, K.L., and McDaniel, P.A.: XAS study of Fe mineralogy in a chronosequence of soil clays formed in basaltic cinders, *Clays Clay Min.*, 58, 772-782, 2010.
- Basler, A., Dippold, M., Helfrich, M., and Dyckmans J.: Microbial carbon recycling-an underestimated
370 process controlling soil carbon dynamics-Part 1: A long-term laboratory incubation experiment, *Biogeosciences*, 12, 5929-5940, 2015.
- Baumgartner, J., Morin, G., Menguy, N., Perez Gonzalez, T., Widdrat, M., Cosmidis, J., and Faivre, D.: Magnetotactic bacteria form magnetite from a phosphate-rich ferric hydroxide via nanometric ferric (oxyhydr)oxide intermediates, *Proc. Natl. Acad. Sci.*, 110, 14883-14888, 2013. Chen, C.M., Dynes,
375 J.J., Wang, J., Karunakaran, C., Sparks, D.L.: Soft X-ray spectromicroscopy study of



- mineral-organic matter associations in Pasture soil clay fractions, *Environ. Sci. Technol.*, 48, 6678-6686, 2014.
- Childs, C.W., Inoue, K., Seyama, H., Soma, M., Theng, B.K.G., and Yuan, G.: X-ray photoelectron spectroscopic characterization of Silica Springs allophane, *Clay Min.*, 32, 565-572, 1997.
- 380 Crist, B.V.: Handbook of monochromatic XPS spectra, XPS International, LLC, Mountain View, USA, 2000.
- Gerin, P., Genet, M., Herbillon, A., Delvaux, B.: Surface analysis of soil material by X-ray photoelectron spectroscopy, *Eur. J. Soil Sci.*, 54, 589-604, 2003.
- Hatton. P.J., Remusat, L., Zeller, B., Derrien, D. A multi-scale approach to determine accurate
385 elemental and isotopic ratios by nano-scale secondary ion mass spectrometry imaging, *Rap. Commu. Mass Spectro.*, 26, 1363-1371, 2012.
- Hatton. P.J., Castanha, C., Torn, M.S., and Bird, J.A.: Litter type control on soil C and N stabilization dynamics in a temperate forest, *Glob. Chang. Biol.*, 21, 1358-1367, 2015.
- Hernandez, Z., Almendros, G., Carral, P., Alvarez, A., Knicker, H., Perez-Trujillo, J.P.: Influence of
390 non-crystalline minerals in the total amount, resilience and molecular composition of the organic matter in volcanic ash soils (Tenerife Island, Spain), *Eur. J. Soil Sci.*, 63, 603-615, 2012.
- Hernes, P.J., Kaiser, K., Dyda, R.Y., Cerli, C.: Molecular trickery in soil organic matter: hidden lignin, *Environ. Sci. Technol.*, 47, 9077-9085, 2013.
- Herrmann, A.M., Ritz, K., Nunan, N., Clode, P.L., Pett-Ridge, J., Kilburn, M.R., Murphy, D.V.,
395 O'Donnell, A.G., Stockdale, E.A.: Nano-scale secondary ion mass spectrometry-A new analytical



- tool in biogeochemistry and soil ecology: A review article, *Soil Biol. Biochem.*, 39, 1835-1850, 2007.
- Hochella, M.F.Jr., Lower, S.K., Maurice, P.A., Penn, R.L., Sahai, N., Sparks, D.L., and Twining, B.S.: Nanominerals, mineral nanoparticles, and Earth systems, *Science*, 319, 1631-1635, 2008.
- 400 Huang, C.C., Liu, S., Li, R.Z., Sun, F.S., Zhou, Y., and Yu, G.H.: Spectroscopic evidence of the improvement of reactive iron mineral content in red soil by long-term application of swine manure, *PLoS One*, 11, e0146364, 2016.
- Kaiser, K., and Guggenberger, G.: Mineral surfaces and soil organic matter, *Eur. J. Soil Sci.*, 54, 219-236, 2003.
- 405 Kögel-Knabner, I., Guggenberger, G., Kleber, M., Kandeler, E., Kalbitz, K., Scheu, S., Eusterhues, K., and Leinweber, P.: Organo-mineral associations in temperate soils: Integrating biology, mineralogy, and organic matter chemistry, *J. Plant Nutr. Soil Sci.*, 171, 61-82, 2008.
- Kramer, M.G., Sanderman, J., Chadwick, O.A., Chorover, J., Vitousek, P.M.: Long-term carbon storage through retention of dissolved aromatic acids by reactive particles in soil, *Glob. Chang. Biol.*, 18, 410 2594-2605, 2012.
- Lalonde, K., Mucci, A., Ouellet, A., Gelinas, Y.: Preservation of organic matter in sediments promoted by iron, *Nature*, 483, 198-200, 2012.
- Li, W., Joshi, S.R., Hou, G.J., Burdige, D.J., Sparks, D.L., and Jaisi, D.P.: Characterizing phosphorus speciation of Chesapeake Bay sediments using chemical extraction, ^{31}P NMR, and X-ray absorption 415 fine structure spectroscopy, *Environ. Sci. Technol.*, 49, 203-211, 2015.



- Liang, B., Lehmann, J., Solomon, D., Sohi, S., Thies, J.E., Skjemstad, J.O., Luizao, F.J., Engelhard, M.H., Neves, E.G., and Wirick, S.: Stability of biomass-derived black carbon in soils, *Geochim. Cosmochim. Acta*, 72, 6069-6078, 2008.
- Mikutta, R., Schaumann, G.E., Gildemeister, D., Bonneville, S., Kramer, M.G., Chorover, J., Chadwick, 420 O.A., and Guggenberger, G.: Biogeochemistry of mineral-organic associations across a long-term mineralogical soil gradient (0.3-4100kyr), Hawaiian Islands, *Geochim. Cosmochim. Acta*, 73, 2034-2060, 2009.
- Mitsunobu, S., Shiraishi, F., Makita, H., Orcutt, B.N., Kikuchi, S., Jorgensen, B.B., Takahashi, Y.: Bacteriogenic Fe(III) (oxyhydr)oxides characterized by synchrotron microprobe coupled with 425 spatially resolved phylogenetic analysis, *Environ. Sci. Technol.*, 46, 3304-3311, 2012.
- Mueller, C.W., Kölbl, A., Hoeschen, C., Hillion, F., Heister, K., Herrmann, A.M., and Kögel-Knabner, I.: Submicron scale imaging of soil organic matter dynamics using NanoSIMS-From single particles to intact aggregates, *Org. Geochem.*, 42, 1476-1488, 2012.
- Parfitt, R.L.: Allophane and imogolite: role in soil biogeochemical processes, *Clay Min.*, 44, 135-155, 430 2009.
- Philippe, A. and Schaumann, G.E.: Interactions of dissolved organic matter with natural and engineered inorganic colloids: A review, *Environ. Sci. Technol.*, 48, 8946-8962, 2014.
- Prietzl, J., Thieme, J., Eusterhues, K., and Eichert, D.: Iron speciation in soils and soil aggregates by synchrotron-based X-ray microspectroscopy (XANES, μ -XANES), *Europ. J. Soil Sci.*, 58, 435 1027-1041, 2007.



- Ramos, M., Ferrer, D., Martinez-Soto, E., Lopez-Lippmann, H., Torres, B., Berhault, G., and Chianelli, R.R.: In-situ HRTEM study of the reactive carbide phase of Co/MoS₂ catalyst, *Ultramicroscopy*, 127, 64-69, 2013.
- Remusat, L., Hatton, P.J., Nico, P.S., Zeller, B., Kleber, M., Derrien, D.: NanoSIMS study of organic matter associated with soil aggregates: advantages, limitations, and combination with STXM, *Environ. Sci. Technol.*, 46, 3943-3949, 2012.
- Rumpel, C., Baumann, K., Remusat, L., Dignac, M.F., Barré, P., Deldicque, D., Glasser, G., Lieberwirth, I., and Chabbi, A.: Nanoscale evidence of contrasted processes for root-derived organic matter stabilization by mineral interactions depending on soil depth, *Soil Biol. Biochem.*, 85, 82-88, 2015.
- Schmidt, M.W.I., Torn, M.S., Abiven, S., Dittmar, T., Guggenberger, G., Janssens, I.A., Kleber, M., Kögel-Knabner, I., Lehmann, J., Manning, D.A.C., Nannipieri, P., Rasse, D.P., Weiner, S., Trumbore, S.E.: Persistence of soil organic matter as an ecosystem property, *Nature*, 478, 49-56, 2011.
- Schumacher, M., Christl, I., Scheinost, A.C., Jacobsen, C., Kretzschmar, R.: Chemical heterogeneity of organic soil colloids investigated by scanning transmission X-ray microscopy and C-1s NEXAFS microspectroscopy, *Environ. Sci. Technol.*, 39, 9094-9100, 2005.
- Senn, A.C., Kaegi, R., Hug, S.J., Hering, J.G., Mangold, S., and Voegelin, A.: Composition and structure of Fe(III)-precipitates formed by Fe(II) oxidation in water at near-neutral pH: Interdependent effects of phosphate, silicate and Ca, *Geochim. Cosmochim. Acta*, 162, 220-246,



- 2015.
- Solomon, D., Lehmann, J., Harden, J., Wang, J., Kinyangi, J., Heymann, K., Karunakaran, C., Lu, Y.,
Wirick, S., and Jacobsen, C.: Micro-and nano-environments of carbon sequestration: Multi-element
STXM-NEXAFS spectromicroscopy assessment of microbial carbon and mineral associations,
460 Chem. Geol., 329, 53-73, 2012.
- Torn, M.S., Trumbore, S.E., Chadwick, O.A., Vitousek, P.M., and Hendricks, D.M.: Mineral control of
soil organic carbon storage and turnover, Nature, 389, 170-173, 1997.
- Xiao, J., Wen, Y.L., Li, H., Hao, J.L., Shen, Q.R., Ran, W., Mei, X.L., He, X.H., Yu, G.H.: In situ
visualisation and characterisation of the capacity of highly reactive minerals to preserve soil organic
465 matter (SOM) in colloids at submicron scale, Chemosphere, 138, 225-232, 2015.
- Vogel, C., Mueller, C.W., Hoschen, C., Buegger, F., Heister, K., Schulz, S., Schloter, M., and
Kögel-Knabner, I.: Submicron structures provide preferential spots for carbon and nitrogen
sequestration in soils, Nat. Commun., 5, 2947, 2014.
- Wen, Y.L., Li, H., Xiao, J., Wang, C., Shen, Q.R., Ran, W., He, X.H., Zhou, Q.S., and Yu, G.H.:
470 Insights into complexation of dissolved organic matter and Al(III) and nanominerals formation in
soils under contrasting fertilizations using two-dimensional correlation spectroscopy and high
resolution-transmission electron microscopy techniques, Chemosphere, 111, 441-449, 2014a.
- Wen, Y.L., Xiao, J., Li, H., Shen, Q.R., Ran, W., Zhou, Q.S., Yu, G.H., and He, X.H. Long-term
fertilization practices alter aluminum fractions and coordinate state in soil colloids, Soil Sci. Soc.
475 Am. J., 78, 2083-2089, 2014b.



- Wild, B., Schnecker, J., Alves, R.J.E., Barsukov, P., Bárta, J., Čapek, P., Gentsch, N., Gittel, A.,
Guggenberger, G., Lashchinskiy, N., Mikutta, R., Rusalimova, O., Šantrůčková, H., Shibistova, O.,
Urich, T., Watzka, M., Zrazhevskaya, G., and Richter, A.: Input of easily available organic C and N
stimulates microbial decomposition of soil organic matter in arctic permafrost soil, *Soil Biol.*
480 *Biochem.*, 75, 143-151, 2014.
- Wu, J., Wu, M.J., Li, C.P., Yu, G.H.: Long-term fertilization modifies the structures of soil fulvic acids
and their binding capability with Al, *PloS one*, 9, e105567, 2014.
- Yaron-Marcovich, D., Chen, Y., Nir, S., and Prost, R.: High resolution electron microscopy structural
studies of organo-clay nanocomposites, *Environ. Sci. Technol.*, 39, 1231-1238, 2005.
- 485 Yu, G.H., Wu, M.J., Wei, G.R., Luo, Y.H., Ran, W., Wang, B.R., Zhang, J.C., and Shen, Q.R.: Binding
of organic ligands with Al(III) in dissolved organic matter from soil: implications for soil organic
carbon storage, *Environ. Sci. Technol.*, 46, 6102-6109, 2012.
- Zhu, T., Lu, X., Liu, H., Li, J., Zhu, X., Lu, J., and Wang, R.: Quantitative X-ray photoelectron
spectroscopy-based depth profiling of bioleached arsenopyrite surface by *Acidithiobacillus*
490 *ferrooxidans*, *Geochim. Cosmochim. Acta*, 127, 120-139, 2014.



Figure Captions

Fig. 1. High-resolution transmission electron microscopy (HRTEM) images of highly reactive minerals from colloids extracted from soil (Ferralic Cambisol) from three long-term (1990-2014) fertilization treatments. (a), TEM images; (b), HRTEM images and selected area electron diffraction (SAED) patterns of the two regions indicated by the blue squares, showing that the black region is a complete crystalline, while the grey region is amorphous; (c-d) energy dispersive X-ray analysis (EDX) images of the region 1 and region 2. Control, no fertilization; NPK, chemical nitrogen, phosphorus and potassium fertilization; NPKM, chemical NPK plus swine manure fertilization.

Fig. 2. Representative NanoSIMS images of $^{12}\text{C}^-$, $^{27}\text{Al}^{16}\text{O}^-$ and $^{56}\text{Fe}^{16}\text{O}^-$ in soil colloids from three contrasting long-term (1990-2014) fertilization treatments (Control, no fertilization, $28 \times 28 \mu\text{m}^2$; NPK, chemical nitrogen, phosphorus and potassium fertilization, $30 \times 30 \mu\text{m}^2$; NPKM, chemical NPK plus swine manure fertilization, $25 \times 25 \mu\text{m}^2$). Note that the color intensity calibration bar displayed in the chemical maps corresponds to the relative concentrations of individual elements, but cannot be used to compare one element with another. Bar = $5 \mu\text{m}$.

Fig. 3. Box plots of $^{12}\text{C}^-/^{27}\text{Al}^{16}\text{O}^-$ (a, b) and $^{12}\text{C}^-/^{56}\text{Fe}^{16}\text{O}^-$ (c, d) ratios reflecting the $^{12}\text{C}^-$ rich ROIs (a, c) and $^{12}\text{C}^-$ less rich ROIs (b, d) of the soil colloids from three contrasting long-term (1990-2014) fertilization treatments using NanoSIMS (for all spots). Control, no fertilization; NPK, chemical nitrogen, phosphorus and potassium fertilization; NPKM, chemical NPK plus swine manure fertilization.

The $^{12}\text{C}^-$ rich ROIs include the areas above 90 pixels and the $^{12}\text{C}^-$ less rich ROIs include the areas in the range of 90-40 pixels under Control and NPK, which were above 50 pixels and in the range of 50-30



pixels under NPKM. The number n in figures represents the number of the selected ROIs. The line in the middle of the box is the median value and the square in the box is the mean value. The lines that protrude out of the boxes represent the 25th and 75th population percentiles. Outliers are shown as
515 diamonds.

Fig. 4. XPS peak-fitting (Al $2p_{3/2}$, C 1s) images recorded from soil (Ferralic Cambisol) colloids extracted under three long-term (1990-2014) fertilization treatments. Control, no fertilization; NPK, chemical nitrogen, phosphorus and potassium fertilization; NPKM, chemical NPK plus swine manure fertilization.

520 **Fig. 5.** Fe K-edge XANES spectra of reference materials and soil colloids from three contrasting long-term (1990-2014) fertilization treatments. The scattered circles represent the linear combination fitting (LCF) results of the sample spectra. Control, no fertilization; NPK, chemical nitrogen, phosphorus and potassium fertilization; NPKM, chemical NPK plus swine manure fertilization.

Fig. 6. Fe K-edge EXAFS (left) and Fourier transforms (right) of reference materials and soil colloids
525 from three contrasting long-term (1990-2014) fertilization treatments. Control, no fertilization; NPK, chemical nitrogen, phosphorus and potassium fertilization; NPKM, chemical NPK plus swine manure fertilization.



Table Captions

Table 1. Basic physiochemical characteristics of soil samples from three contrasting long-term
530 (1990-2014) fertilization treatments ^a.

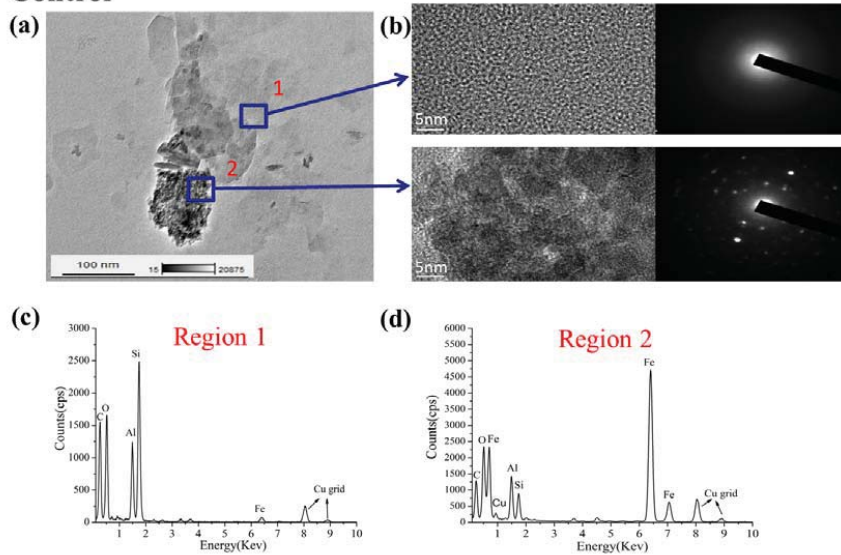
Table 2. Binding energy and quantitation/assignment of XPS spectral bands of soil samples from three
contrasting long-term (1990-2014) fertilization treatments ^a.

Table 3. Linear combination fit (LCF) results of Fe K-edge XANES spectra of the soil colloids from
three contrasting long-term (1990-2014) fertilization treatments ^a.

535

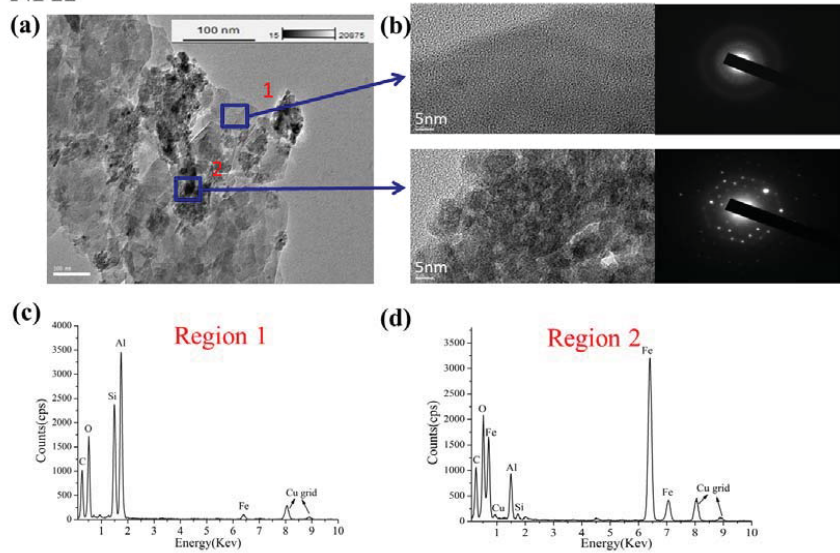


Control





NPK



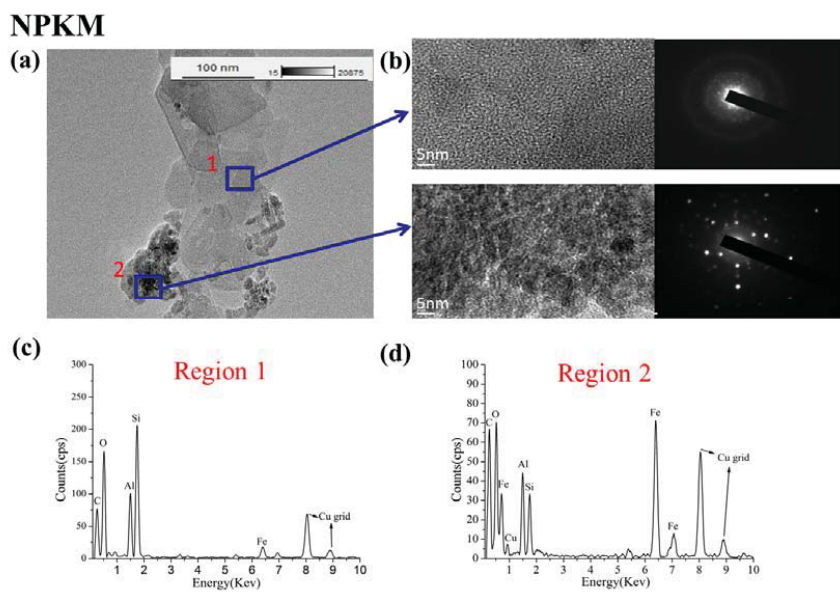
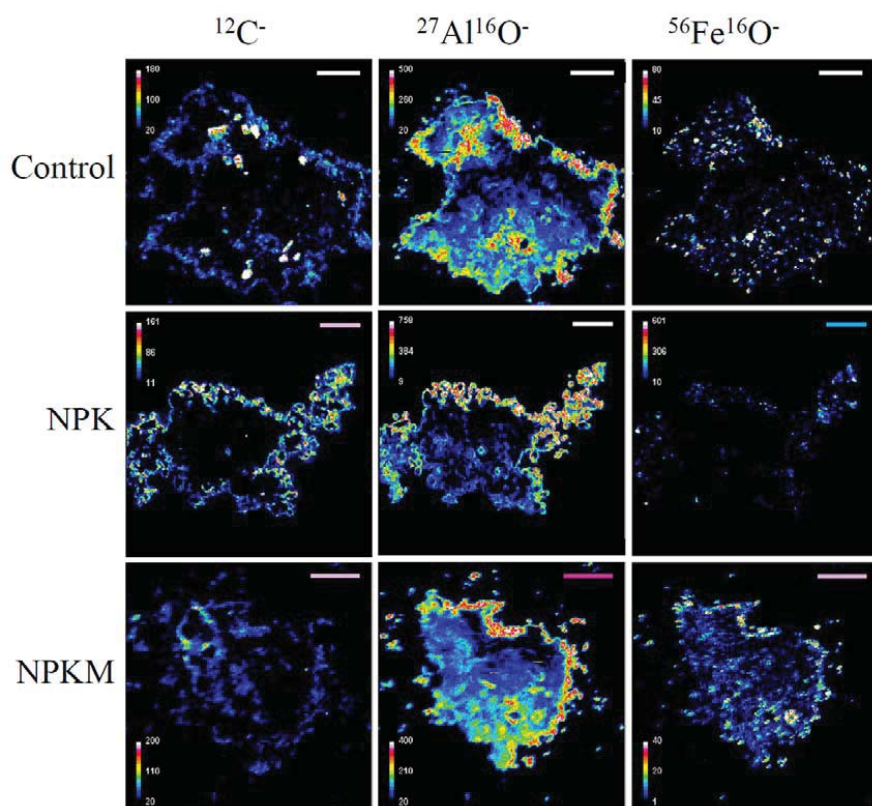


Figure 1



540

Figure 2

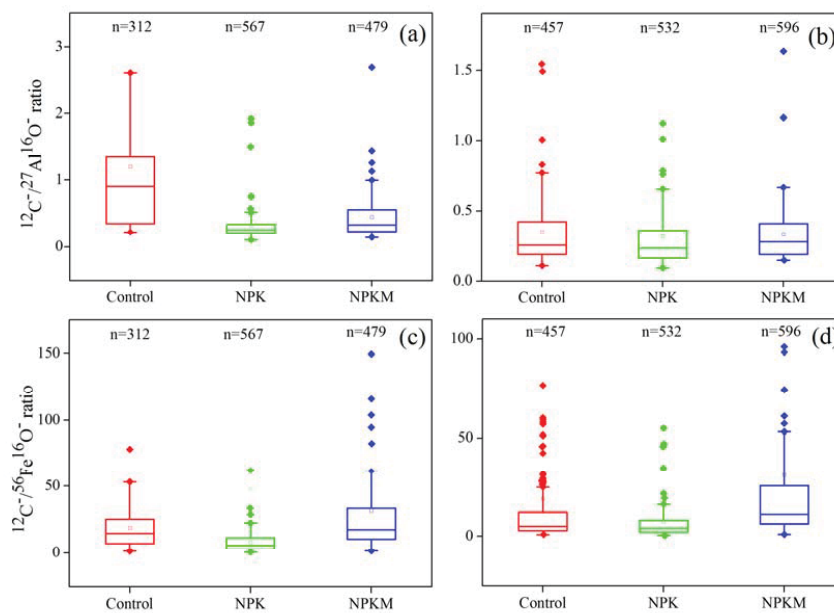


Figure 3

545

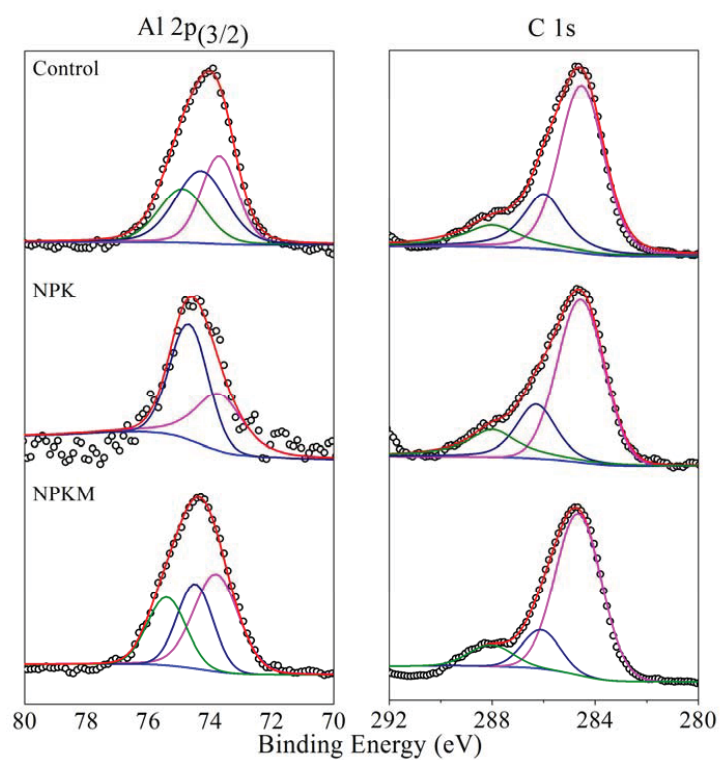


Figure 4

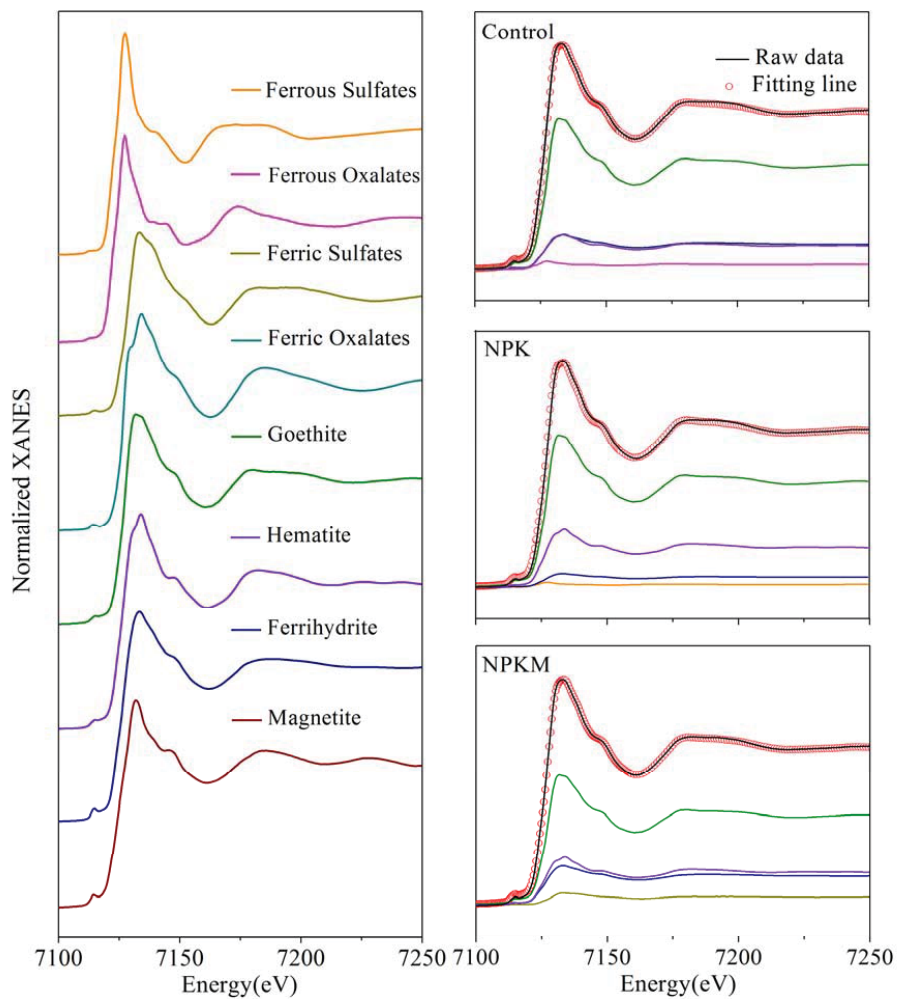


Figure 5

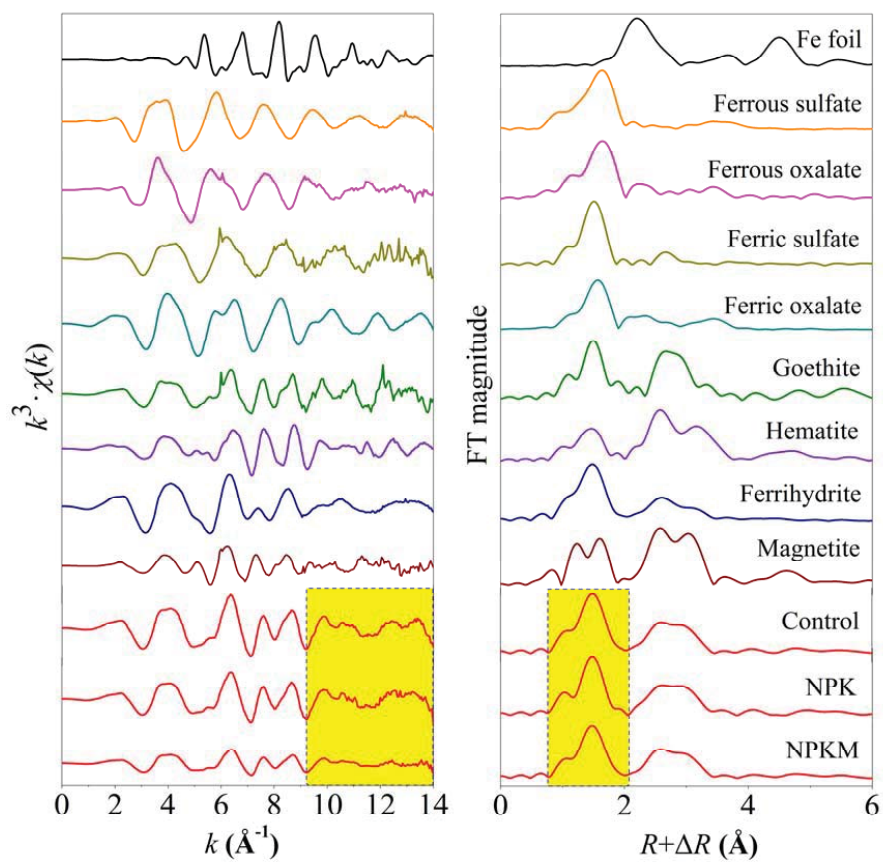


Figure 6

553 **Table 1. Basic physiochemical characteristics of soil samples from three separate long-term (1990-2014) fertilization treatments ^a.**

Treatment	Soil					Soil colloids				
	pH	SOM (g kg ⁻¹)	Al _o (%)	Fe _o (%)	SRO (%)	Al _{XPS} (%)	Fe _{XPS} (%)	DOC (mg L ⁻¹)	DOC/Al _{XPS}	DOC/Fe _{XPS}
Control	5.47 ± 0.04b	14.88 ± 2.02c	0.07 ± 0.003b	0.20 ± 0.004b	0.17 ± 0.00b	6.23	1.47	6.17	0.99	4.20
NPK	4.15 ± 0.00c	18.36 ± 0.16b	0.04 ± 0.003c	0.16 ± 0.003c	0.12 ± 0.00c	1.22	0.48	4.62	3.79	9.63
NPKM	5.84 ± 0.01a	25.13 ± 2.02a	0.11 ± 0.002a	0.30 ± 0.007a	0.26 ± 0.01a	6.84	1.59	42.02	6.14	26.43

554 ^a Note: Control, no fertilization; NPK, chemical nitrogen, phosphorus and potassium fertilization; NPKM, chemical NPK plus swine manure
 555 fertilization, SOM, soil organic matter. Al_{XPS} and Fe_{XPS} indicated the surface concentration of Al and Fe in soil colloids, which were determined
 556 by the X-ray photoelectron spectroscopy (XPS). Al_o and Fe_o indicated reactive Al and Fe nanominerals, which were extracted using acid
 557 ammonium oxalate. DOC, dissolved organic carbon in soil colloids. Short-range ordered (SRO) minerals were calculated using the formula of
 558 Al_o + 1/2 Fe_o (%) (Kramer et al., 2012). Significant differences among fertilization treatments were determined using one-way ANOVA followed
 559 by the Tukey's HSD post hoc test at $P < 0.05$ after the conditions of normality and homogeneity of variance were met.

560



561 **Table 2. Binding energy and quantitation/assignment of XPS spectral bands of soil samples from three separate long-term (1990-2014)**
 562 **fertilization treatments^a.**

Element	Control			NPK			NPKM		
	Peak (eV)	Atomic (%)	Assignment	Peak (eV)	Atomic (%)	Assignment	Peak (eV)	Atomic (%)	Assignment
Al 2p _{3/2}	73.8	34.2	Allophane Al ₂ O ₃ / Al ₂ O ₃ -nH ₂ O	73.8	42.9	Allophane Al ₂ O ₃ / Al ₂ O ₃ -nH ₂ O	73.8	45.1	Allophane Al ₂ O ₃ / Al ₂ O ₃ -nH ₂ O
Al 2p _{3/2}	74.3	39.0	Boehmite AlO(OH)	74.7	57.1	Boehmite AlO(OH)	74.5	29.4	Boehmite AlO(OH)
Al 2p _{3/2}	74.9	26.8	AlOx	/	/	/	75.4	25.5	AlOx
C 1s	284.6	62.3	Aromatic carbon (Ar-C-C/Ar-C-H)	284.6	62.5	aromatic carbon (Ar-C-C/Ar-C-H)	284.6	75.9	aromatic carbon (Ar-C-C/Ar-C-H)
C 1s	286.1	23.6	Ether or alcohol carbon (C-O)	286.2	20.8	Ether or alcohol carbon (C-O)	286.1	14.7	Ether or alcohol carbon (C-O)
C 1s	288.0	14.2	Ketonic or aldehyde carbon (C=O)	288.0	16.7	Ketonic or aldehyde carbon (C=O)	288.0	9.5	Ketonic or aldehyde carbon (C=O)

563 ^aNote: Control, no fertilization; NPK, chemical nitrogen, phosphorus and potassium fertilization; NPKM, chemical NPK plus swine manure
 564 fertilization. The atomic percentage (%) is the corrected value calculated from the XPS peak-fitting areas (Childs et al., 1997; Crist, 2000) and
 565 elemental assignments were determined from published studies (Liang et al., 2008; Mikutta et al., 2009; Xiao et al., 2015).

566



567 **Table 3. Linear combination fit (LCF) results of Fe K-edge XANES spectra of the soil colloids from three separate long-term (1990-2014)**
 568 **fertilization treatments ^a.**

Treatment	LCF results (%)						LCF parameters	
	Goethite	Hematite	Ferrihydrite	Ferric sulfates	Ferrous citrates	Ferrous sulfates	R-factor	Chi-square
Control	66.0 ± 0.025	14.9 ± 0.000	16.0 ± 0.025	ND	3.10 ± 0.012	ND	0.000052	0.00437
NPK	67.0 ± 0.025	25.0 ± 0.000	6.30 ± 0.020	ND	ND	1.70 ± 0.008	0.000051	0.00426
NPKM	56.8 ± 0.025	20.4 ± 0.000	18.0 ± 0.017	4.8 ± 0.018	ND	ND	0.000051	0.00436

569 ^a Note: Control, no fertilization; NPK, chemical nitrogen, phosphorus and potassium fertilization; NPKM, chemical NPK plus swine manure

570 fertilization. ND, not detected. Determination of parameters of fit (i.e., R-factor and chi-square) indicated that the LCF results are convincing.